# Developing and Testing of a Generic Micro-CHP Model for Simulations of Dwellings and Highly Distributed Power Systems

N. J. Kelly[1#], J. A. Clarke[1], A. Ferguson[2] and G. Burt[3]

[1]Energy Systems Research Unit, University of Strathclyde, Glasgow, UK

[2] Sustainable Buildings and Communities Group, Natural Resources Canada, Ottawa

[3] Institute for Energy and Environment, University of Strathclyde, Glasgow, UK

## ABSTRACT

This paper elaborates an approach to the modelling of domestic micro combined heat and power (μ-CHP) using a building simulation tool that can provide a detailed picture of the environmental performance of both the μ-CHP heating system and the dwelling it serves. The approach can also provide useful data for the modelling of highly distributed power systems. However, at the commencement of the work no μ-CHP device model that was compatible with a building simulation tool was available. The development of such a model is described along with its calibration and verification.

The simulation tool with the device model was then applied to the analysis of a dwelling with a Stirling engine-based heating system. Different levels of thermal insulation and occupancy types were modelled. The energy and environmental performance of the μ-CHP device was quantified for each case; additionally, the potential for its participation in the control and operation of a highly distributed power system (HDPS) was assessed.

---

[#] Corresponding author: Energy Systems Research Unit, University of Strathclyde, 75 Montrose St. Glasgow G11XJ, e-mail: nick@esru.strath.ac.uk

Analysis of the simulation results indicated that the parasitic losses associated with the μ-CHP system balance of plant reduced the overall heating system efficiency by up to 40%. Performance deteriorated with increasing levels insulation in the dwelling, resulting in reduced thermal efficiency and increased cycling, though overall fuel use was reduced. The analysis also indicated that in the device was generally available to participate in HDPS control for above 90% of the simulation time. The potential length of participation time ranged from 1 to 800+ minutes and depended upon the state of the μ-CHP system thermal buffer and prevailing heat loads. Probabilities for different participation times and modes were calculated.

*Keywords*: micro-CHP, building simulation model, highly distributed power system.

## 1 BACKGROUND

The drive towards low or even zero carbon buildings in the UK and the emergence of domestic micro-generation over the last decade is changing the way in which we think about buildings as an energy system. Previously, buildings were seen as passive consumers of energy – consuming fossil fuels and drawing power from the grid to meet the needs of the occupants with respect to heating, cooling, lighting and ventilation. However, the prospect is now emerging of buildings producing part or all of their own (significantly reduced) energy needs, or even exporting electrical energy to the grid.

The concept of the Highly Distributed Power System (HDPS) has appeared in response to the emergence of micro-generation. The HDPS is a move away from the current electricity system model of a few large generators feeding many loads towards a model of many smaller generators feeding many loads [1]. Such profound changes in built environment energy systems and equally profound changes in the electricity

system pose significant engineering challenges. Pertinent research issues range from optimising the thermal and electrical performance of micro-generation devices in dwellings through to assessing the fundamental stability and security of a power system featuring a diverse range of small generators.

Micro combined heat and power (μ-CHP) is one of the low carbon micro-generation technologies which could be installed in buildings in very large numbers and so could play a important part in the operation of any future HDPS. The technologies underpinning μ-CHP include Stirling engines (SE), fuel cells and internal combustion engines (ICE). While fuel cell μ-CHP is still an embryonic technology, the development of engine-based systems has progressed rapidly in recent years. Dentice d'Accadia *et al* [2] identified 12 different units at various stages of commercialisation, with sizes ranging from 1-15 kW of electrical output and 3-39 kW of thermal output. Both Honda and SenerTec [3] are marketing residential-scale ICE μ-CHP devices.

Despite the proliferation of the technology and its entry into the market place, it is by no means certain that the installation of a μ-CHP unit within a building will result in significant emissions savings. Several recent studies have addressed this issue [4,5 & 6] indicating that achieving tangible carbon savings with μ-CHP is dependent upon many factors including the operation and control of the unit, the prevailing climate, the behaviour of the building occupants and the magnitude of the heat and power demands. Indeed the studies by Peacock and Newborough [5] and Kelly and Cockroft [6] indicated that under certain circumstances $CO_2$ emissions may *increase* with the installation of μ-CHP. All of these studies relied on simplified models of both the building and the associated micro-CHP device. Typically, the building was represented by fixed heat and power demand profiles and fixed efficiencies were assumed for the μ-CHP.

This paper reports modelling work undertaken within two research projects: the Supergen Highly Distributed Power Systems Consortium (www.supergen-hdps.org) and the International Energy Agency's Energy (IEA) Conservation in Building and Community Systems (ECBCS) Annex 42 (www.cogen-sim.net) [7]. The modelling approach differs significantly from the efforts mentioned previously in that the dwelling and μ-CHP system are represented explicitly using a mathematical model developed on a building simulation platform - ESP-r [8]. This model uses real climate data, information on occupancy patterns and user-defined control criteria as the boundary conditions to predict the dynamic performance of the building and associated energy systems. At the level of an HDPS the model can generate credible time series electrical power production profiles that can be used a boundary condition for the prediction of electrical network performance. At the level of the individual dwelling, the model provides an appropriate platform with which to evaluate not only likely carbon savings from μ-CHP but also to explore subtle nuances of performance such as rates of on/off switching, temporal variations in efficiency and interactions with thermal storage and other balance of plant all under realistic operating conditions.

The paper concludes with an analysis of a typical UK dwelling equipped with μ-CHP device and a hydronic heating system. The analysis covers the energy and environmental performance of the device along with its likely participation of the micro-generation device in the operation of an HDPS.

## 2 A GENERIC MICRO-CHP MODEL

From an end-users perspective, the main requirement for a μ-CHP model is to accurately predict the time-varying thermal and electrical outputs and their explicit interaction the building's envelope, thermal plant, and control systems. The important

elements that need to be simulated are therefore the variables that couple the μ-CHP device model to the other constituents of a building simulation model, specifically the heat output (hot water), electrical power output and heat losses. Further, from a performance and environmental perspective, the fuel consumption needs to be accurately predicted.

Analysis of performance data from several μ-CHP units coupled with extensive model development and testing work within IEA ECBCS Annex 42 [7, 9] has indicated that the generic form of model shown in Figure 1 is appropriate for the simulation of μ-CHP devices; this was developed using a pragmatic "grey box" modelling approach, where the model structure partially reflects the underlying physical device.

<<figure 1 here>>

The engine unit is represented as a single functional block with a series of inputs and outputs; these are linked by a performance map (a series of parametric equations linking the inputs of the model to the outputs). In addition, the heat output passed to a lumped-capacitance thermal model, featuring two thermal control volumes, which are added to enable the transient thermal performance of the engine unit and coupled heat exchange equipment (engine jacket and exhaust gas heat exchanger) to be adequately modelled. These are:

- the *thermal mass control volume* that (roughly) represents the aggregated thermal capacitance associated with the engine block and the majority of the heat exchanger shells; and
- the *cooling water control volume* that represents the cooling water flowing through the device and the elements of the heat exchanger in immediate thermal contact.

The need for two control volumes emerged from the analysis of the thermal response of both Stirling and ICE engine units. In both cases the cooling water outlet temperature (this is the coupling point between the device and the rest of an integrated model) exhibited rapid changes to variations in coolant flow rate and temperature and much slower response to changes in engine loading. The two-volume model can adequately represent both of these responses.

### 2.1 Performance Map

In the performance map, the engine's steady-state (part load) performance is correlated to the total energy input to the system:

$$P_{net,ss} = \eta_e q_{gross} \quad (1)$$

$$q_{gen,ss} = \eta_q q_{gross} \quad (2)$$

$$q_{gross} = \dot{m}_{fuel} \cdot LHV_{fuel} \quad (3)$$

The cogeneration system's part load electrical and thermal efficiencies, ($\eta_e$, $\eta_q$ [-]), are determined using empirical correlations relating the conversion efficiencies to the flow rate and temperature of cooling water, and the unit's electrical loading:

$$\eta_e = f(\dot{m}_{cw}, T_{cw}, P_{net,ss}) \quad (4)$$

and

$$\eta_q = f(\dot{m}_{cw}, T_{cw}, P_{net,ss}) \quad (5)$$

Effectively, this performance map describes the cogeneration system's steady-state behaviour under a variety of loading conditions.

The full performance map expression for electrical efficiency is as follows:

$$\begin{aligned}\eta_e = {} & a_0 + a_1 P_{net,ss}^2 + a_2 P_{net,ss} \\ & + a_3 \dot{m}_{cw}^2 + a_4 \dot{m}_{cw} \\ & + a_5 T_{cw}^2 + a_6 T_{cw} \\ & + a_7 P_{net,ss}^2 \dot{m}_{cw}^2 + a_8 P_{net,ss} \dot{m}_{cw} + a_9 P_{net,ss} \dot{m}_{cw}^2 + a_{10} P_{net,ss}^2 \dot{m}_{cw} \\ & + a_{11} P_{net,ss}^2 T_{cw}^2 + a_{12} P_{net,ss} T_{cw} + a_{13} P_{net,ss} T_{cw}^2 + a_{14} P_{net,ss}^2 T_{cw} \\ & + a_{15} \dot{m}_{cw}^2 T_{cw}^2 + a_{16} \dot{m}_{cw} T_{cw} + a_{17} \dot{m}_{cw} T_{cw}^2 + a_{18} \dot{m}_{cw}^2 T_{cw} \\ & + a_{19} P_{net,ss}^2 \dot{m}_{cw}^2 T_{cw}^2 + a_{20} P_{net,ss}^2 \dot{m}_{cw}^2 T_{cw} + a_{21} P_{net,ss}^2 \dot{m}_{cw} T_{cw}^2 + a_{22} P_{net,ss} \dot{m}_{cw}^2 T_{cw}^2 \\ & \quad + a_{23} P_{net,ss}^2 \dot{m}_{cw} T_{cw} + a_{24} P_{net,ss} \dot{m}_{cw}^2 T_{cw} + a_{25} P_{net,ss} \dot{m}_{cw} T_{cw}^2 \\ & \quad + a_{26} P_{net,ss} \dot{m}_{cw} T_{cw}\end{aligned} \quad (6)$$

Similarly for thermal efficiency:

$$\begin{aligned}\eta_q = {} & b_0 + b_1 P_{net,ss}^2 + b_2 P_{net,ss} \\ & + b_3 \dot{m}_{cw}^2 + b_4 \dot{m}_{cw} \\ & + b_5 T_{cw}^2 + b_6 T_{cw} \\ & + b_7 P_{net,ss}^2 \dot{m}_{cw}^2 + b_8 P_{net,ss} \dot{m}_{cw} + b_9 P_{net,ss} \dot{m}_{cw}^2 + b_{10} P_{net,ss}^2 \dot{m}_{cw} \\ & + b_{11} P_{net,ss}^2 T_{cw}^2 + b_{12} P_{net,ss} T_{cw} + b_{13} P_{net,ss} T_{cw}^2 + b_{14} P_{net,ss}^2 T_{cw} \\ & + b_{15} \dot{m}_{cw}^2 T_{cw}^2 + b_{16} \dot{m}_{cw} T_{cw} + b_{17} \dot{m}_{cw} T_{cw}^2 + b_{18} \dot{m}_{cw}^2 T_{cw} \\ & + b_{19} P_{net,ss}^2 \dot{m}_{cw}^2 T_{cw}^2 + b_{20} P_{net,ss}^2 \dot{m}_{cw}^2 T_{cw} + b_{21} P_{net,ss}^2 \dot{m}_{cw} T_{cw}^2 + b_{22} P_{net,ss} \dot{m}_{cw}^2 T_{cw}^2 \\ & \quad + b_{23} P_{net,ss}^2 \dot{m}_{cw} T_{cw} + b_{24} P_{net,ss} \dot{m}_{cw}^2 T_{cw} + b_{25} P_{net,ss} \dot{m}_{cw} T_{cw}^2 \\ & \quad + b_{26} P_{net,ss} \dot{m}_{cw} T_{cw}\end{aligned} \quad (7)$$

Where $a_0$–$a_{26}$ (-) and $b_0$–$b_{26}$ (-) are empirically-derived coefficients. Many of these coefficients reduce to zero after regression analysis for particular devices, however they have been included for completeness.

Note that the efficiency correlations described by equations 6 and 7 quantify the cogeneration system's steady-state and part load performance, and do not characterize its dynamic thermal or electrical behaviour.

### 2.2 Thermal Mass Control Volume

The dynamic thermal behaviour of the a combustion-based cogeneration device is characterized by the thermal mass of its engine block and encapsulated working fluid, internal heat exchange equipment; these are represented using a single, homogeneous thermal mass control volume. The thermal energy stored within this control volume is quantified using an aggregate thermal capacitance, $[MC]_{eng}$, (J/K) and an equivalent average engine temperature $T_{eng}$ ($^{o}$C).

The energy balance of the thermal mass control volume shown in figure 1 is:

$$[MC]_{eng}\frac{dT_{eng}}{dt} = q_{gen,ss} - q_{HX} - q_{skin-loss} \quad (8)$$

#### 2.2.1 Cooling water control volume

The energy balance of the cooling water control volume shown in figure 1 is:

$$[MC]_{cw}\frac{T_{cw,o}}{dt} = [\dot{m}c_p]_{cw}\left(T_{cw,i} - T_{cw,o}\right) + q_{HX} \quad (9)$$

Heat is transferred to the cooling water from the exhaust gases and the engine casing. The rate of heat recovery may differ from the calculated steady-state rate of recoverable heat production ($q_{gen,ss}$) due to:

- the thermal mass of the engine and other heat transfer components , which store some of the recoverable heat produced within the engine, and
- the effects of internal controllers regulating phenomena such as of exhaust-gas recirculation and the operation of an external heater in Stirling engines.

The heat transfer between the engine and the cooling water control volume is quantified using an overall heat-transfer coefficient:

$$q_{HX} = UA_{HX}\left(T_{eng} - T_{cw,o}\right) \quad (10)$$

It is assumed that the heat lost from the engine is proportional to the temperature difference between the engine and the surroundings. Thus:

$$q_{skin-loss} = UA_{loss}\left(T_{eng} - T_{room}\right) \quad (11)$$

where $UA_{loss}$ (W/K) is the effective thermal conductance between the engine control volume and the surroundings.

Using Equations 10 and 11, the engine and cooling water control volume energy balance equations (Equations 8 and 9) can be rewritten:

$$[MC]_{eng}\frac{dT_{eng}}{dt} = UA_{HX}\left(T_{cw,o} - T_{eng}\right) + UA_{loss}\left(T_{room} - T_{eng}\right) + q_{gen,ss} \quad (12)$$

$$[MC]_{cw}\frac{T_{cw,o}}{dt} = [\dot{m}c_p]_{cw}\left(T_{cw,i} - T_{cw,o}\right) + UA_{HX}\left(T_{eng} - T_{cw,o}\right) \quad (13)$$

## 3 MODEL CALIBRATION

Calibration of the parameters for this model is a two stage process. The first stage is to produce the performance maps that characterise the performance at different operational states: different loading levels (where appropriate), cooling water flow rates and temperatures. The main function of the performance map is to predict the heat transferred to the cooling system of the unit; it is also used to predict the unit's fuel consumption.

### 3.1 Dynamic Calibration

The second stage of the calibration process was to tune the characteristics ($MC_{eng}$, $MC_{cw}$, $UA_{HX}$ and $UA_{loss}$) of the dynamic thermal model using data from dynamic tests on the μ-CHP unit; these tests could cover periods when the unit is in start-up or shut down mode and/or when the thermal or electrical load on the unit is changed.

The necessary performance maps (equations 6 and 7) were developed by regression analysis using data from laboratory tests in which the μ-CHP unit was tested at various load levels and cooling water flow rates.

Calibration of the dynamic elements of the model (control volumes) required an iterative parameter identification procedure using the GenOpt optimization utility (Wetter [10]); this is designed to determine the parameter set providing the minimum value of a specified cost function; in this case this is the average error between the measured cooling water outlet temperature and the value predicted by the model:

$$E = \frac{1}{N}\sum_{i=1}^{i=N} e_i \qquad (25)$$

Here, $e_i$ is the error at each simulation time step and $N$ is the number of simulation time steps in the optimisation simulation.

### 3.2 Stirling Engine Calibration and Validation

Calibration of the Stirling Engine was undertaken by Ferguson [9] using the two-stage process described with data collected by Entchev et al. [11], who installed a small, Stirling CHP unit an experimental test house at the Canadian Centre for Housing Technology (CCHT), and measured its performance when subjected to simulated thermal loads. This data set was split into two: one set was used for calibration and the other for verification of the model's predictions. The Stirling μ-CHP unit used in this study exhibited relatively low electrical efficiency (8-9% LHV), and a high heat-to-power ratio (9:1). The unit had a 750We electrical output and was capable of producing around 7 kW of heat. The device was regulated using an on-off controller and exhibited nearly constant fuel flow and electrical output when operating.

Figure 2 plots the Stirling μ-CHP model's predictions against experimental data for a two-hour test period. In this test, the unit was started from cold and the coolant flow rate perturbed. The test was replicated with the model and the results indicate that it can adequately represent the dynamic performance of the unit.

<<figure 2 here>>

### 3.3 ICE Calibration

A similar process was undertaken to calibrate the model to steady-state and dynamic performance data from a Senertec ICE unit. This unit has different characteristics to the Stirling Engine in that it has a peak electrical power output of 5 kW and a thermal output of 14.5 kW. The predictions of the calibrated model in comparison to experimental tests (in which the unit is switched on and off and the coolant flow rate is varied) are shown in figure 3. Again, this shows that the calibrated generic model gives a good prediction of the dynamic thermal performance of this μ-CHP device.

<<figure 3 here>>

## 4 CASE STUDY

Using the building simulation tool equipped with the μ-CHP device model the energy and environmental performance (e.g. $CO_2$ emissions and fuel consumption) of a Stirling engine-based domestic heating system was determined when integrated into a detached dwelling. Further, as befits the detailed nature of the model developed, more fine-grained performance data was also examined: on/off cycling, transient thermal performance, the impact of balance of plant and the temporal characteristics of electrical output. Using this information, the potential for the μ-CHP to actively participate with the local electrical network in areas such as voltage control was assessed.

### 4.1 Integrated Model

*Building Fabric*

The ESP-r building model was developed from various analyses of the UK housing stock [12,13,14] and comprises a representation of the building geometry coupled with explicit representations of the different constructions, occupancy characteristics, temporal hot water draws along with space and water heating control requirements. The total floor area of the dwelling is 136 $m^2$.

Table 1 shows the 'U-values' associated with the main constructions that were used with the model. The lower U-value constructions are representative of older housing in the current UK stock. The higher U-values were taken from the "passivehausUK" (www.passivhaus.org.uk) specifications; these were also associated with significantly reduced infiltration, and mechanical ventilation with heat recovery was integrated into

the model when they were used. These two levels of insulation bracket the range of dwelling fabric types within which a μ-CHP unit could be expected to operate.

*Occupancy*

The dwelling model was populated by a four-person family. Corresponding detailed daily heat gain profiles (covering weekdays and weekends) for people and equipment based on continuous occupancy and intermittent occupancy were developed based on the work of Jardine [15].

*Heating System*

The detailed model of the heating system, which was integrated with the building model is shown in figure 4. The μ-CHP unit was coupled to the rest of the heating system via a 200*l* buffer tank featuring an internal heat exchanger: this fed both the radiators and the domestic hot water tank and buffers the μ-CHP unit from the instantaneous space heat and hot water demands, reducing the need for *on/off* cycling. The core of the system and the buffer tank capacity is typical of that seen in demonstration installations for μ-CHP, e.g. Entchev et al. [11].

<<figure 4 here>>

The μ-CHP unit was controlled using an on/off controller with a 10$^{o}$C dead-band. Control was based on the buffer tank temperature, which was maintained between 65 and 75$^{o}$C during heating periods. The hot water storage tank was controlled to maintain a water supply temperature of approximately 50$^{o}$C by regulating the flow of hot water from the buffer tank into the hot water tank's heat exchanger. The draws on the hot water tank were generated using the IEA model developed by Jordan and Vajen [16]. This has been validated against monitored European hot water demand profiles [17].

## 4.2 Simulations

Four variants of the dwelling model were developed featuring different combinations of fabric insulation and occupancy. For each, two simulations were run representing a typical heating season week in winter and the transition seasons (spring/autumn). These used a London data set (the reference UK dynamic climate for building simulations). Each simulation was conducted using a 5-minute time step, enabling the dynamics associated with the thermal inertia of components and the operation of the various controllers in the dwelling's heating system to be captured.

The simulations run are labelled as follows:

- transition #11 – transition week, poorly insulated, continuous occupancy;
- winter #11– winter week, poorly insulated, continuous occupancy;
- transition #12 – transition week, poorly insulated, intermittent occupancy;
- winter #12 – winter week, poorly insulated, intermittent occupancy;
- transition #21 – transition week, well insulated, continuous occupancy;
- winter #21– winter week, well insulated, continuous occupancy;
- transition #22 – transition week, well insulated, intermittent occupancy;
- winter #22 – winter week, well insulated, intermittent occupancy;

### 4.3 Results

Figure 5 gives a sample of some of the large quantity of detailed, dynamic performance information available from the building simulations. It shows the water temperature in the buffer tank, the associated μ-CHP electrical power output and the temperature in the living room of the dwelling over the course of a simulated week. For this paper, systems-level summary performance metrics have been extracted from the detailed simulation data. This is presented in tables 2-6. These tables summarise the overall energy performance of the μ-CHP system and characterise some of the temporal characteristics relevant to its mechanical performance and availability to provide services to the local electrical network.

<<figure 5 here>>

### 4.4 Discussion of Results

*Energy and Environmental Performance*

The impact of adequately insulating the building reduced the space heating requirements by up to 60% and also had a significant impact on the effectiveness of the Stirling μ-CHP system. In all of the simulations the basic device efficiency was extremely good, ranging from 88% up to 95%. The higher device efficiencies occurred during the winter week, and corresponded to the heaviest heat loading. Unit efficiencies fell in the transition week and also as the insulation level of the dwelling increased; this was due to greater unit cycling frequencies and a reduction in the time in which the unit was producing power.

The overall system efficiency was significantly lower than the device efficiency. For example in the poorly insulated dwelling, system efficiencies ranged from 9-28% below the unit efficiency, this was caused by non-useful ‘parasitic’ heat losses from

the buffer tank, hot water tank and piping. The effect was even more pronounced for the well-insulated dwelling, with system efficiencies ranging from 18 to 40% lower than the device efficiency. The poorest performance occurred during the transition week, when the useful heat load was reduced in comparison to the parasitic losses: in this situation more heat was lost from the tanks and piping than was usefully delivered to the space. In winter this effect was less pronounced as the space heating demands were higher.

It is interesting to note that the high μ-CHP device and system efficiencies occurred in the 'winter #11' and 'winter #12' simulations for the poorly insulated dwelling. However, closer inspection of the simulation results indicated that the heating system supply and hot water tank temperatures were often lower than the required system set point temperatures and so the system heat losses were lower than would otherwise be the case. Hence, although the derived efficiency was high, the system failed to deliver enough heat to provide thermal comfort in the dwelling at certain times. The same problem occurred (though to a lesser extent) in the transition #12 simulation.

*Temporal Characteristics*

The mode of operation, the season and insulation levels had a significant impact on the temporal characteristics of the μ-CHP system heat and power output. For example, the number of times the unit cycled over the simulated week varied significantly between simulations. When serving the continuously occupied, poorly insulated dwelling over a winter week the system operated with 11, long *on* periods averaging 799 minutes, punctuated by short *standby* periods averaging 119 minutes. Improving the dwelling insulation levels caused a reduction in the length of each *on* period to an average of 222 minutes with a corresponding increase in the length of *standby* periods to an average 247 minutes over 21 cycles. Clearly, minimising the

cycling frequency would be beneficial to the longevity of the μ-CHP device and would reduce maintenance.

When heavily loaded, the unit tended to operate for long periods on full power in an attempt to maintain the buffer tank temperature within the operating range of 65-75$^{o}$C. However, with a lighter heat load the buffer tank reached its operating conditions more quickly and then the μ-CHP unit cycled to stay within the temperature range. The number of cycles was similar for each transition period simulation (transition #11 and #21). However, the average unit *on* time was reduced from an average of 296 minutes to 157 minutes with better dwelling insulation levels.

The number of operational cycles and their length directly affected the amount of power produced by the μ-CHP unit. As the heat demand fell so did the potential for electricity cogeneration, for example during the winter week the electrical output of the Stirling unit was 118 kWh however this dropped to 57 kWh for the better-insulated case.

When the heating system was operated intermittently in winter to complement an intermittent occupancy, the number of cycles did not vary between simulations. The constrained unit operation time resulted in the unit being *on* when the control regime allowed as between the intermittent firing, the buffer tank temperature fell below the minimum set point temperature of 65$^{o}$C due to parasitic heat losses. Hence, in the next operational period the unit needed to fire continuously to bring the tank temperature back into the operating range.

When operated intermittently during the transition season, the level of insulation in the dwelling caused significant changes in operational times: with poor insulation the unit was operational for 40% of the time, improving the insulation levels on the

dwelling reduced this to 25% of the time, with a corresponding reduction in electrical production from 48kWh to 31kWh. The difference was far less pronounced for the winter simulation. Operational times only fell from 40% to 38%. This was symptomatic of the intermittent control rather than a true reflection of the effect of insulating the dwelling. As was mentioned previously, for the poorly insulated, intermittent winter case (winter #12), the μ-CHP system struggled to achieve the operating temperature range in the buffer tank, so the actual operating time would have been significantly longer than the 40% observed if the device had not been constrained by the control settings.

*Availability for Participation in HDPS Control*

The ability to externally control a μ-CHP device to meet some network need could be an important element in the safe and reliable operation of an HDPS. However the ability of the device to respond to such a need is heavily constrained by the thermal demands of its client building. The data from the simulation results was analysed to give an indication of likely ability of the μ-CHP to respond to an external network control signal. For the non-modulating device modelled, three responses to external requests for control were possible:

1. If the buffer tank temperature was below its upper limit of 75$^{o}$C and the device is *off* then the it could be switched *on* to provide power to the network (i.e. to counteract a drop in the network voltage) until the upper temperature limit of the buffer tank was reached – *positive participation*.
2. If the buffer tank temperature was above its lower limit of 65$^{o}$C and the device was *on* then it could be switched *off* (to counteract a network voltage rise) until the buffer tank temperature fell to its lower limit – *negative participation*.

3. Finally if the device was *on* with a buffer tank temperature of below 65°C or *off* with a buffer tank temperature of above 75°C then the unit was unavailable for use in network control as the dwelling's thermal needs had priority - *unavailable.*

Note that in cases 1 and 2 the thermal loads in the dwelling would continue to be served by the buffer tank and were be unaffected by the external control of the unit.

Table 6 shows the resulting μ-CHP device availabilities from each simulation - typically above 90%. However, in cases where the device struggled to meet the heat load (the poorly insulated dwelling in winter) availability reduced to around 60% as the device would often was *on* with a buffer tank temperature of below 65°C. The participatory mode was influenced by the level of insulation: in the well insulated 'Passivehaus' dwelling availability for negative participation (i.e. switching off) was markedly less than for the poorly insulated dwelling (figure 7) due to the smaller dwelling heat load and reduced run time for the unit. Conversely, scope for positive HDPS participatory (switching on from standby) control was increased.

*Determining the Duration of Participation*

An analysis of the buffer tank thermal characteristics from the simulations indicated that its typical cool down time from 75°C to 65°C was around 800 minutes. The heating time between the same temperature bands was approximately 200 minutes. Using this information it was possible to derive the approximate time for positive or negative participation of the μ-CHP device for any point in time during a simulation.

Figure 6 is typical of the results emerging from this analysis and shows the probability for different positive participation duration times occurring over a transition week for both the poorly insulated and well-insulated dwelling. Possible participation times

ranged from 1 to 200+ minutes. However, increasing the insulation levels significantly increased the probability of participation times lasting less than 100 minutes.

<<figure 6 here >>

Figure 7 shows the corresponding probabilities for negative participation for different participation duration times, which ranged from 1 to 800+ minutes. These were significantly lower over the spectrum of duration times than was the case for positive participation. Increasing insulation levels reduced these probabilities further.

<<figure 7 here>>

## 5 CONCLUSIONS

This paper has described the development and testing of a generic μ-CHP device model for use in integrated simulations of domestic energy systems. The model uses a modified performance-map to enable the calculation of the part load performance. This is combined with a dynamic thermal model comprising two lumped thermal masses enabling the device model to adequately capture the dynamic variations of the cooling water temperature: the critical thermal coupling variable between the device, heating system and client building. The model has been calibrated to represent both Stirling and internal combustion engine-based μ-CHP devices.

Poorly insulated and well-insulated model variants of a UK detached dwelling have been developed, complete with a detailed model of the heating system, micro-CHP device and control settings and the occupancy derived heat gains. Dynamic thermal simulations using this model indicated a significant drop in efficiency (up to 40%) when the device was coupled to a heating system and operated in a realistic context.

The performance of the micro-CHP system deteriorated when dwelling insulation levels were improved. However, reduced heat demands led to an overall reduction in carbon emissions. Better dwelling insulation also reduced the electrical power produced by the unit and therefore the potential to displace grid electricity or export power to the grid.

When considering the potential for provision of network services from the micro-CHP device it was found that the device was generally available around 90% of the time to respond to a request from the network service in cases where the device struggled to meet the thermal load of the dwelling. In these cases availability was significantly lower.

The device could switch *off* in response to an external control signal for between 1 to 800+ minutes and switch *on* for between 1 to 200+ minutes. In both cases the maximum response time depended upon the tank temperature and prevailing heat loads. Improving the insulation level of the dwelling significantly increased the availability of the device to switch *on* and provide power to the network (i.e. to raise voltage levels). The availability of the device to a switch *off* signal from the network remained low for both the well insulated and poorly insulated cases.

Finally, the results from the simulations demonstrated the strong couplings between the μ-CHP system, the balance of plant and the load thus emphasising the value of fully integrated modelling as described in this paper.

### 5.1 Further Work

This paper here has dealt mainly with the development of a generic μ-CHP device model and its application to a limited range of scenarios. The conclusions from this analysis are therefore limited to the specific device modelled and to its operational

context. The device model and building simulation will be applied to a much broader range of devices, dwellings, climates and operational scenarios to produce a more comprehensive picture of performance in the UK housing stock as a whole.

## 6 ACKNOWLEDGEMENTS

The model development and calibration described in this paper was undertaken as part of the International Energy Agency's Energy Conservation in Building and Community Systems research Annex 42: The Simulation of Building- Integrated Fuel Cell and Other Cogeneration Systems (www.cogen-sim.net). The Annex is an international collaborative research effort and the authors gratefully acknowledge the indirect or direct contributions of the other Annex participants.

The simulation work described in this paper was undertaken within the SuperGen Highly Distributed Power Systems consortium. The authors gratefully acknowledge the funding and support of the UK Engineering and Physical Sciences Research Council and the indirect or direct contributions of the other consortium members.

## 7 NOMENCLATURE

| | |
|---|---|
| $\eta_e$ | the steady-state electrical conversion efficiency of the engine (-) |
| $\eta_q$ | the steady-state part load, thermal efficiency of the engine (-) |
| $LHV_{fuel}$ | the lower heating value of the fuel used by the system (J/kg or J/kmol) |
| $\dot{m}_{fuel}$ | the fuel flow rate (kg/s or kmol/s), |
| $\dot{m}_{cw}$ | the mass flow rate of the cooling water (kg/s) |

$T_{cw}$ the temperature of the cooling water at the inlet of the cooling water control volume ($^{o}$C).

$k_f$ an empirical coefficient (-)

$\dot{m}_{fuel,warm-up}$ the rate of fuel flow during warm-up (kg/s)

$\dot{m}_{fuel,ss-max}$ (kg/s) the maximum rate of fuel flow to the device under steady-state conditions (kg/s)

$\dot{m}c_{p\,cw}$ the thermal capacity flow rate associated with the cooling water (W/K)

$MC_{eng}$ the thermal capacitance of the control volume (W/K)

$MC_{cw}$ the thermal capacitance of the encapsulated cooling water and heat exchanger shell in immediate thermal contact (J/K)

$P_{net,ss}$ is the rate of steady-state electricity production (W)

$q_{gen,ss}$ the steady-state rate of heat generation within the engine (W)

$q_{gross}$ is the gross heat input into the system (W)

$q_{HX}$ the rate of heat transfer to the cooling water (W)

$q_{skin-loss}$ the rate of heat loss from the unit (W)

$T_{cw,o}$ the bulk exit temperature of the encapsulated cooling water and shell ($^{o}$C)

$T_{cw,i}$ the temperature of the cooling water entering the unit ($^{o}$C)

$T_{eng}$ the bulk temperature of the thermal mass control volume ($^{o}$C)

$t$ time (s)

$T_{eng}$ the average temperature of the engine control volume. ($^{o}$C)

$T_{eng,nom}$ the nominal engine temperature ($^{o}$C)

$UA_{HX}$ the overall thermal conductance between the engine cooling water control volumes (W/K)

## 8 REFERENCES


1 Burt G, 2008. *An Overview of The Highly Distributed Power System Conce*pt, Proc Microgen 2008, The First International Conference and Workshop on Micro-cogeneration and Applications, National Arts Centre, Ottawa, Canada, Apr 29-May 1

2 Dentice d'Accadia M, Sasso M, Sibilio S, Vanoli L, 2003. *Micro-combined heat and power in residential and light commercial applications*, Applied Thermal Engineering, 23 (10) 1247-1259

3 Slowe J, 2008. *International Micro-CHP Review and Outlook*, Proc. Microgen2008, The First International Conference and Workshop on Micro-cogeneration and Applications, National Arts Centre, Ottawa, Canada, Apr 29-May 1

4 Hawkes A D and Leach M A, 2007. *Cost-effective operating strategy for residential micro-combined heat and power*, Energy 32, pp 711-723.

5 Peacock A, Newborough M, 2005. *Impact of micro-CHP systems on domestic sector $CO_2$ emissions*. Applied Thermal Engineering, Volume 25, Issue 17-18, pp 2653-2676.

6 Cockroft J, Kelly N J, 2006. *A Comparative Assessment of Future Heat and Power Sources for the UK Domestic Sector*, Energy Conversion and Management 47, pp 2349-2360.

7 Beausoleil-Morrison I, Kelly N J, eds., 2007. *Specifications for Modelling Fuel Cell and Combustion-Based Residential Cogeneration Device within Whole-Building Simulation Programs*, IEA/ECBCS Annex 42. Available at www.cogen-sim.net.

8 Clarke J A 2001. *Energy Simulation in Building Design*, 2nd Ed, Butterworth-Heineman, London.

9 Beausoleil-Morrison I. and Ferguson A., eds., 2007. *Inter-model Comparative Testing and Empirical Validation of Annex 42 Models for Residential Cogeneration Devices*, IEA/ECBCS Annex 42. Available at www.cogen-sim.net.

10 Wetter M, 2004. *GenOpt(R) Generic Optimization Program*, Lawerence Berkeley National Laboratory, US Deparment of Energy.

11 Entchev E, Gusdorf J, Swinton M, Bell M, Szadkowski F, Kalbfleisch W and Marchand R 2004. Micro-generation technology assessment for housing technology, Energy and Buildings, 36(9), September, pp925-931.

12 Department for Communities and Local Government, English House Condition Survey 2004 (http://communities.gov.uk/ehcs )

13 Communities Scotland, *Scottish House Condition Survey 2002* (revised 2003) (http://www.scotland.gov.uk )

14 Utley J I, Shorrock L, Brown J H F, 2001. *Domestic Energy Fact File: England, Scotland, Wales and Northern Ireland*, BRE Report Available at www.bre.co.uk

15 Jardine C, *Synthesis of High Resolution Domestic Electricity Load Profiles*, 2008. Proc Microgen2008, The First International Conference and Workshop on Micro-cogeneration and Applications, National Arts Centre, Ottawa, Canada, Apr 29-May 1

16 Jordan U and Vajen K 2000. *Influence of the DHW Load Profile on the Fractional Energy Savings: A Case Study of a Solar-combi System with TRNSYS Simulations*, Solar Energy (69), pp 197-208.

17 Knight I and Kreutzer N 2008. *The IEA Annex 42 Non-HVAC Electrical and DHW Consumption Profiles for European Residential Energy Demands*, Proc. Microgen2008, The First International Conference and Workshop on Micro-cogeneration and Applications, National Arts Centre, Ottawa, Canada, Apr 29-May 1

## 9 TABLES

**Table 1**: U-values used in building models.

| **'Base case'** **Construction elements** | **U-value ($W/m^2K$)** | **'Passivhaus'** **Construction elements** | **U-value ($W/m^2K$)** |
|---|---|---|---|
| external wall | 1.42 | external surfaces | 0.15 |
| windows | 2.1 | windows | 0.8 |
| roof (loft insulation) | 0.36 | | |

**Table 2**: energy and environmental metrics for μ-CHP from simulations, poorly-insulated dwelling.

| **Poorly insulated Simulated week** | **Unit eff. (%)** | **Net Power KWh** | **Heat out kWh** | **Losses KWh** | **$CO_2$ kg** | **Space heat kWh** | **Water heat kWh** | **Sys eff. (%)** |
|---|---|---|---|---|---|---|---|---|
| transition #11 | 92 | 73 | 690 | 150 | 186 | 445 | 95 | 74 |
| winter #11 | 95 | 118 | 1025 | 165 | 269 | 768 | 93 | 82 |
| transition #12 | 92 | 48 | 466 | 49 | 126 | 357 | 59 | 83 |
| winter #12 | 92 | 48 | 466 | 39 | 126 | 394 | 32 | 85 |

**Table 3:** energy and environmental metrics for μ-CHP from simulations, well-insulated dwelling over a simulated week.

| Well insulated Simulated week | Unit eff. % | Net Power KWh | Heat out kWh | Losses KWh | $CO_2$ kg | Space heat kWh | Water heat kWh | Sys eff. % |
|---|---|---|---|---|---|---|---|---|
| transition #21 | 88 | 33 | 330 | 167 | 87 | 69 | 94 | 48 |
| winter #21 | 91 | 57 | 544 | 159 | 140 | 292 | 92 | 67 |
| transition #22 | 89 | 31 | 291 | 119 | 76 | 77 | 96 | 57 |
| winter #22 | 91 | 46 | 453 | 100 | 116 | 275 | 78 | 73 |

**Table 4** temporal metrics for μ-CHP from simulations with poorly-insulated dwelling over a simulated week.

| Poorly insulated Simulated week | % of time on/ warmup | % of time standby/ cool down | ave time on mins | ave time Standby Mins | cycles # |
|---|---|---|---|---|---|
| transition #11 | 59 | 41 | 296 | 199 | 20 |
| winter #11 | 87 | 13 | 799 | 119 | 11 |

| | | | | | |
|---|---|---|---|---|---|
| transition #12 | 40 | 60 | 266 | 407 | 15 |
| winter #12 | 40 | 60 | 266 | 407 | 15 |

**Table 5**: temporal metrics for μ-CHP from simulations with well-insulated dwelling over a simulated week.

| **Well insulated**<br><br>**Simulated week** | **% of time**<br>**on/**<br>**warmup** | **% of time**<br>**standby/**<br>**cooldown** | **ave time**<br>**on**<br>**mins** | **ave time**<br>**Standby**<br>**mins** | **cycles**<br><br>**#** |
|---|---|---|---|---|---|
| transition #21 | 28 | 72 | 157 | 403 | 18 |
| winter #21 | 46 | 54 | 222 | 247 | 21 |
| transition #22 | 25 | 75 | 166 | 506 | 15 |
| winter #22 | 38 | 62 | 259 | 414 | 15 |

**Table 6**: Availability of the μ-CHP to participate in HDPS control.

| **Poorly insulated case**<br><br>**Simulated week** | **availability for positive participation**<br>**(% of time)** | **availability for negative participation**<br>**(% of time)** | **unavailable**<br>**(% of time)** |
|---|---|---|---|
| transition #11 | 60 | 32 | 8 |
| winter #11* | 31 | 32 | 37 |
| Transition #12* | 69 | 23 | 8 |
| winter #12* | 62 | 0 | 38 |
| | | | |
| **Well insulated case**<br><br>**Simulated week** | **availability for positive participation**<br>**(% of time)** | **availability for negative participation**<br>**(% of time)** | **unavailable**<br>**(% of time)** |
| transition #21 | 78 | 18 | 4 |
| winter #21 | 64 | 30 | 6 |
| transition #22 | 84 | 10 | 6 |
| winter #22 | 75 | 20 | 5 |

* In these case unit struggled to meet the thermal demand of the dwelling.

**CAPTIONS FOR FIGURES**

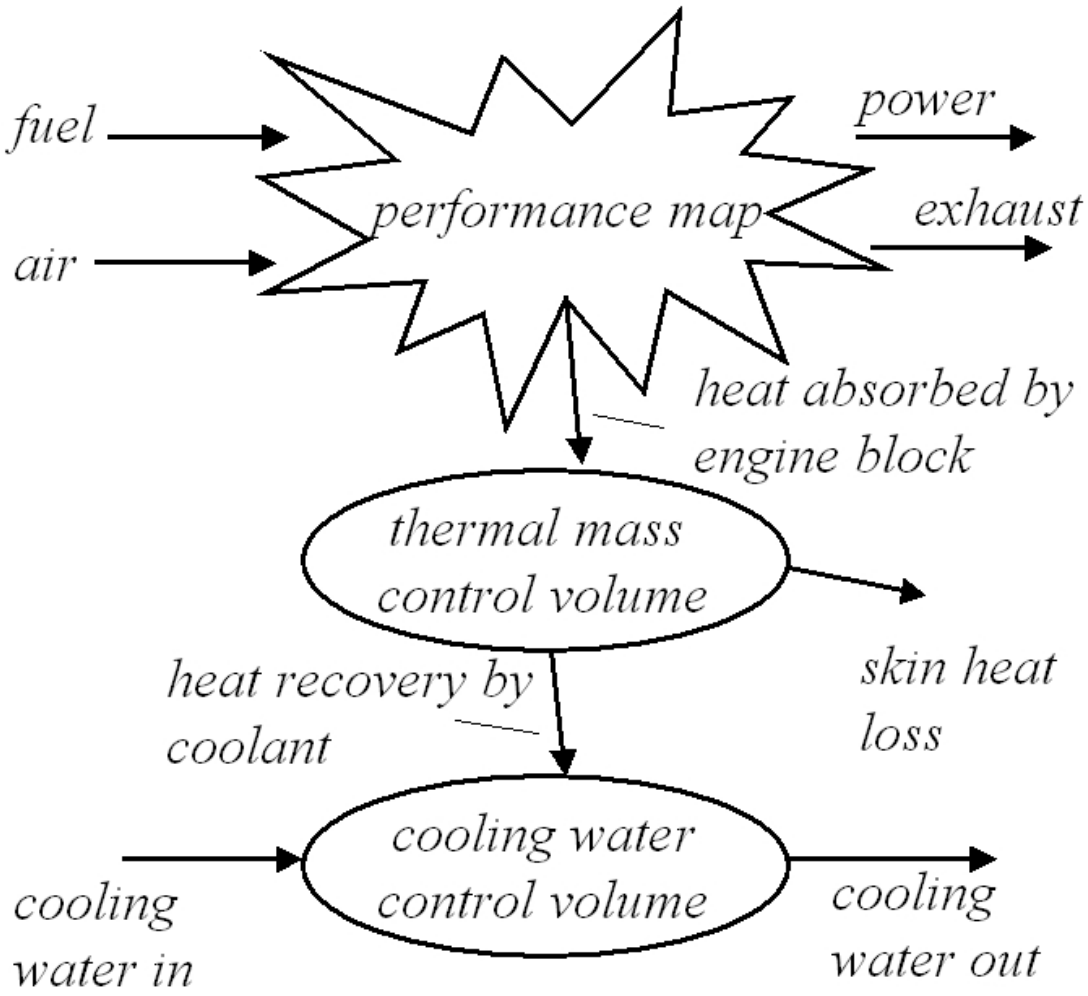


**Figure 1**: The basic form of the μ-CHP device model.

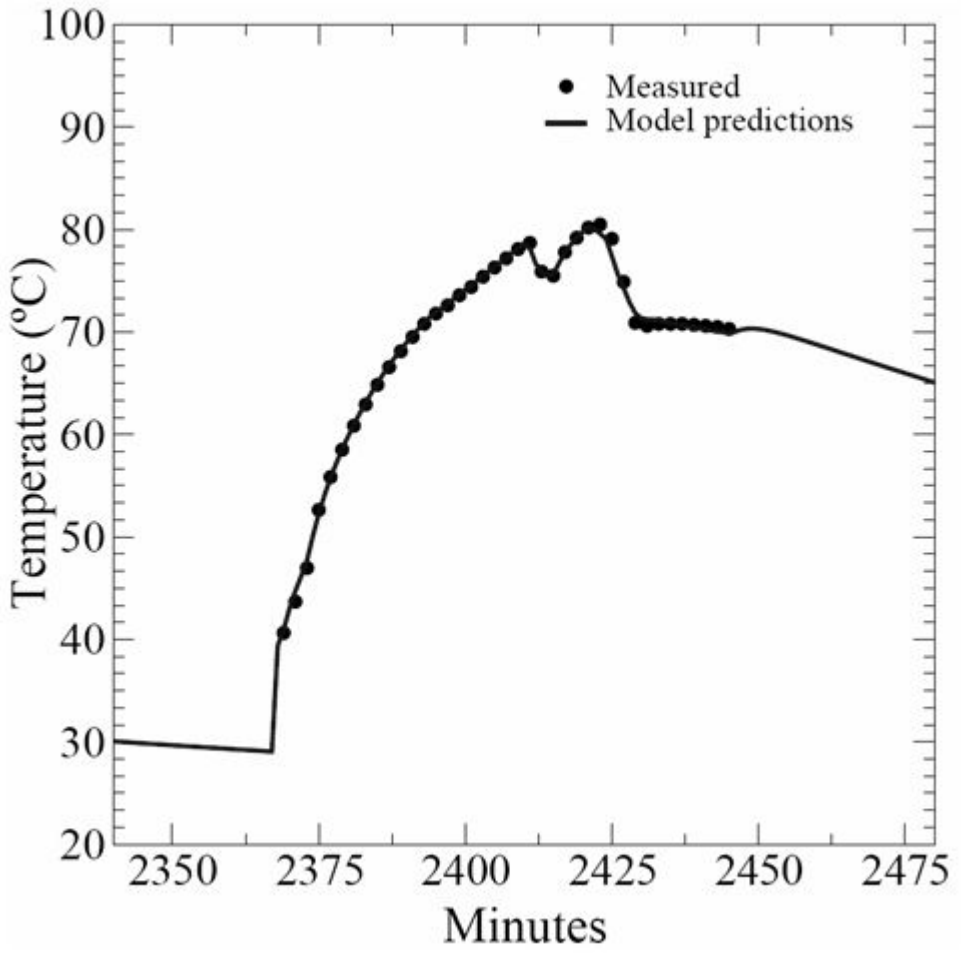


**Figure 2:** Stirling model predictions of cooling water outlet temperature vs. experimental results

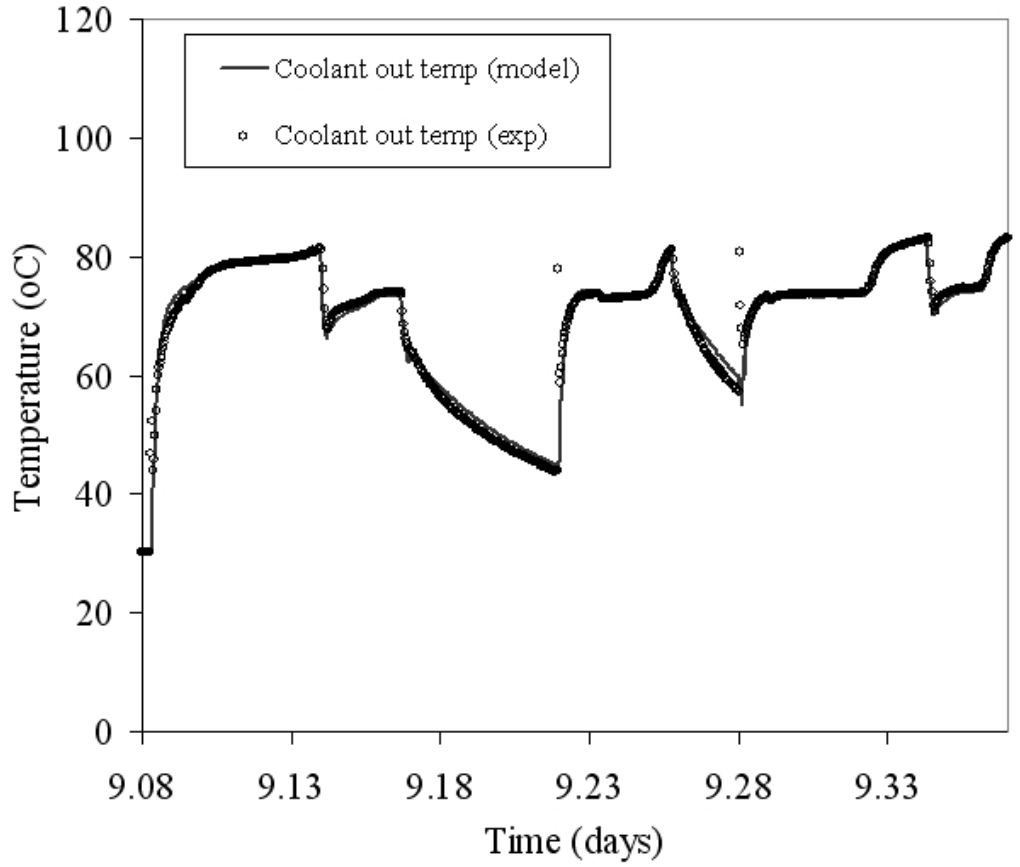


**Figure 3:** ICE model predictions of cooling water temperature vs. experimental results

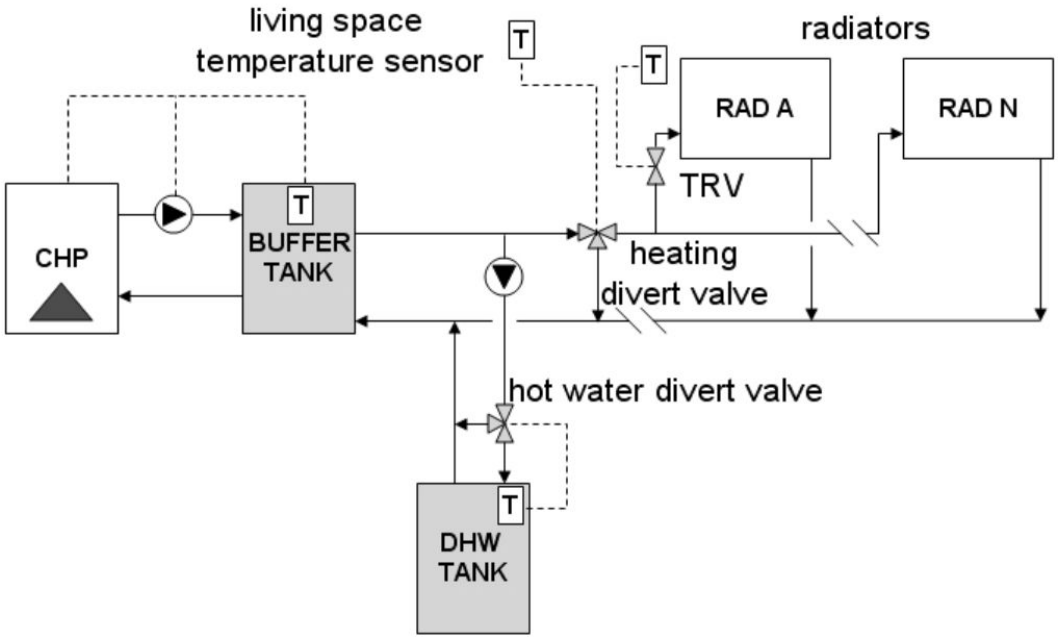


**Figure 4**: Heating system sub-model.

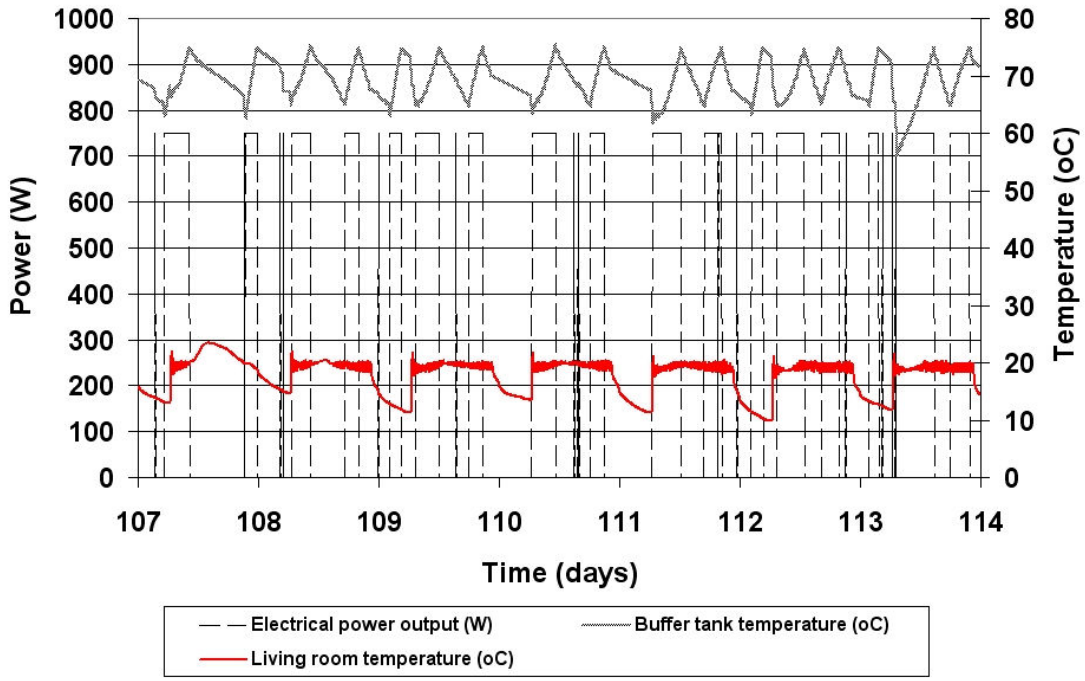


**Figure 5**: Sample of results available from the simulations.

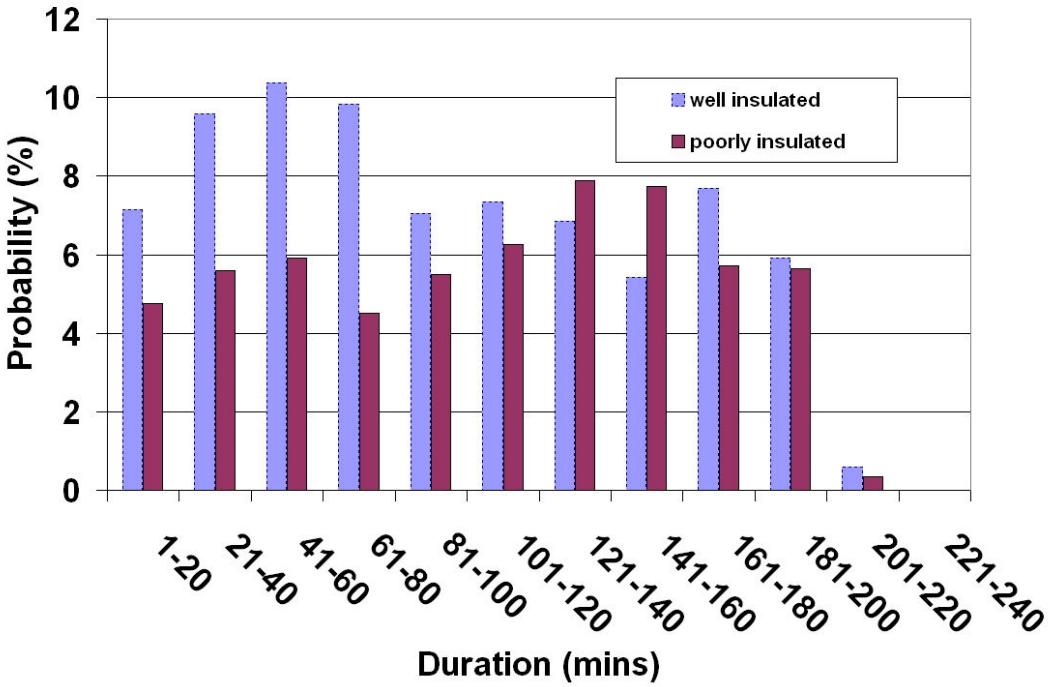


**Figure 6**: Probability of different durations of positive device participation in HDPS control – poorly insulated dwelling, continuously occupied, transition season.

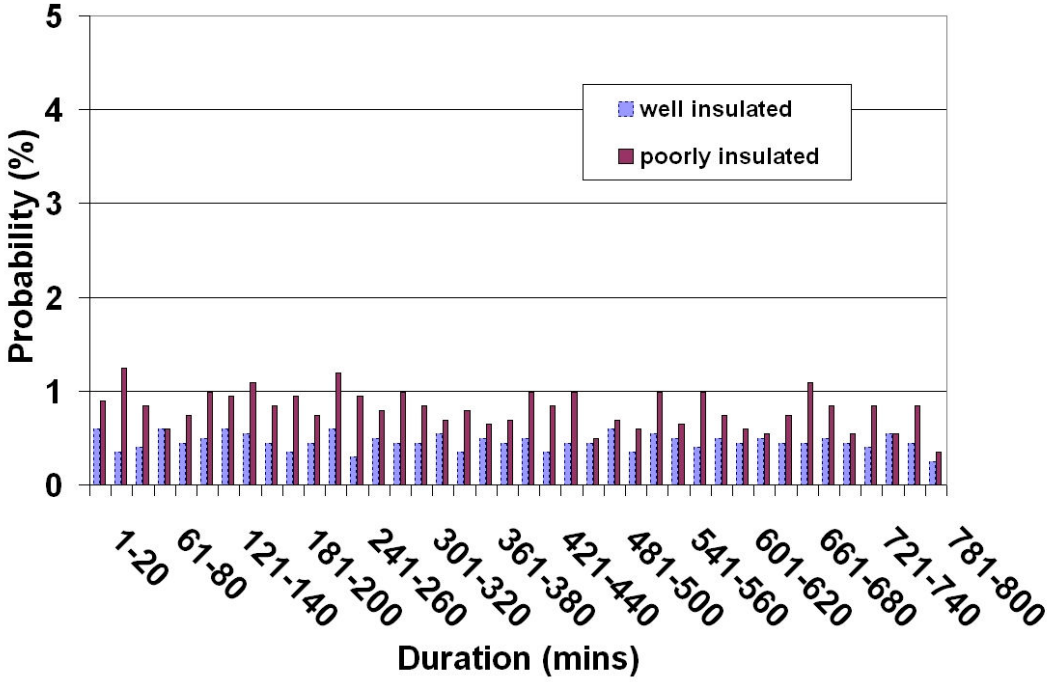


**Figure 7**: Availability of the device to participate in HDPS control – well insulated dwelling, continuously occupied, transition season.